FP7-600716

Whole-Body Compliant Dynamical Contacts in Cognitive Humanoids

D5.3
Validation scenario 3: balancing on compliant environmental contacts

Editor(s)	Daniele Pucci
Responsible Partner	IIT
Affiliations	[1] IIT
Status-Version:	Draft-1.0
Date:	Feb. 28, 2016
EC Distribution:	Consortium
Project Number:	600716
Project Title:	Whole-Body Compliant Dynamical Contacts in Cognitive Humanoids

Title of Deliverable: balancing on compliant environmental contacts	Validation scenario 3:
Date of delivery to the EC:	28/2/2016

Workpackage responsible for the Deliverable	deliv WP5
Editor(s):	Daniele Pucci
Contributor(s):	Daniele Pucci, Francesco Romano, Jorhabib Eljaik, Silvio Traversaro, Vincent Padois, Francesco Nori
Reviewer(s):	
Approved by:	All Partners

Abstract	This deliverable discusses the technical details and choices for the implementation of the year-3 validation scenario of the CoDyCo project. The validation scenario aims at verifying the control performances in the case the humanoid robot iCub must balance by means of compliant or dynamical contacts. With *dynamical contact* we mean that the robot's link in contact with the environment is not fixed with respect to an inertial frame, and the wrench applied to it is not due to a spring-damper system. First, we detail the control algorithm for dealing with a soft carpet underneath the robot's feet. This case study exemplifies the case of a robot interacting with a compliant environment. Then, we present the control algorithm to allow the robot balancing on a semi-cylindrical seesaw. This case study exemplifies the problem of a humanoid robot balancing by means of dynamical contacts. In fact, the robot's feet do not have a constant pose with respect to the inertial frame in this case. Contact and trajectory planning are not part of the scenario.

Keyword List:	Multiple, compliant, dynamical, contacts, control, stability, tracking, forces, torques.

Document Revision History

Version	Date	Description	Author
First draft	19 Feb 2016	In this version we simply write down a few considerations on the third year validation scenario as discussed after the mid-year CoDyCo meeting in Birmingham.	Daniele Pucci

Table of Contents

1 Introduction

Differently from the first and second year validation scenarios, the third year CoDyCo scenario consists in adding compliance and dynamicity of the robot contacts while the humanoid attempts at balancing. This kind of situations have not received much attention from the control community, and the solutions presented in this document are original in several aspects.

As in the previous validation scenarios, the control objective is the regulation of the robot momentum. The rate-of-change of this momentum equals the summation of all external wrenches applied to the system, and controlling the external wrenches to stabilize the robot's momentum is a known control strategy for humanoids when balancing. One of the main difficulties when dealing with compliant and dynamical contacts in this context comes from the fact that the external wrenches may not be instantaneously related to the robot's torques, i.e. the input to the system. This is the case, for instance, of a humanoid standing on two springs, which exert forces on the robot's feet that depend on the relative compressions only.

There may be some particular soft terrains, however, that exert forces and torques not only depending on the relative compressions, but also on the robot's joint torques. In these cases, the soft terrain is subject to some rigid constraints that may allow the control of the robot's momentum through the external forces, which thus depend on the joint torques. This is the case of a thin, highly damped carpet, which can be modeled, in the first approximation, as a continuum of vertical springs. Each of these springs is assumed to compress vertically only, and the other degrees of freedom are rigidly constrained, thus creating the aforementioned relation between external forces and joint torques [**?**]. The first experimental demonstration during the review meeting consists of showing the humanoid robot iCub while it balances on a soft carpet of the above kind.

We then go one step further and present control algorithms to deal with *dynamical* contacts. The application scenario of the controller consists of the humanoid robot iCub balnacing on a semi-cylindrical seesaw. In this case, the contacts between the robot ad its environment are subject to the seesaw dynamics, and the control of the robot is particularly challenging.

The iCub will be torque controlled and the controller assumes that desired torques are exactly executed by a lower level torque control. Dynamics will be computed with a custom library, iDynTree[1], built on top of KDL[2].

The deliverable is organized as follows. Section **??** gives an high level presentation of the validation scenario to be presented at the second year review meeting. Section **??** discusses the numerical technique (TSID) used to implement the validation scenario as a prioritization of concurrent tasks. Section **??** discusses the set of control tasks that will be implemented in order to perform the validation scenario. Their sequencing in the form of a finite state machine is discussed in Section **??** and issues related to task switching discussed in Section **??**.

[1] `http://wiki.icub.org/codyco/dox/html/group__iDynTree.html`
[2] `http://www.orocos.org/kdl`

2 Background

2.1 Notation

Throughout the paper we will use the following definitions:

- $\mathcal{I}$ denotes an inertial frame, with its z axis pointing against the gravity. We denote with g the gravitational constant.
- $e_i \in \mathbb{R}^m$ is the canonical vector, consisting of all zeros but the i-th component which is one.
- Given two orientation frames A and B, and vectors of coordinates expressed in these orientation frames, i.e. ${}^A p$ and ${}^B p$, respectively, the rotation matrix ${}^A R_B$ is such that ${}^A p = {}^A R_B \, {}^B p$.
- $1_n \in \mathbb{R}^{n \times n}$ is the identity matrix of size n; $0_{m \times n} \in \mathbb{R}^{m \times n}$ is the zero matrix of size $m \times n$ and $0_n = 0_{n \times 1}$.
- We denote with $S(x) \in \mathbb{R}^{3 \times 3}$ the skew-symmetric matrix such that $S(x)y = x \times y$, where $\times$ denotes the cross product operator in $\mathbb{R}^3$.

2.2 Robot equations of motion

We assume that the robot is composed of $n+1$ rigid bodies – called links – connected by n joints with one degree of freedom each. In addition, we also assume that the multi-body system is *free floating*, i.e. none of the links has an *a priori* constant pose with respect to the the inertial frame. This implies that the multi-body system possesses $n + 6$ degrees of freedom. The configuration space of the multi-body system can then be characterized by the *position* and the *orientation* of a frame attached to a robot's link – called *base frame* $\mathcal{B}$ – and the joint configurations. More precisely, the robot configuration space is defined by

$$\mathbb{Q} = \mathbb{R}^3 \times SO(3) \times \mathbb{R}^n.$$

An element of the set $\mathbb{Q}$ is then a triplet

$$q = ({}^{\mathcal{I}} p_{\mathcal{B}}, {}^{\mathcal{I}} R_{\mathcal{B}}, q_j),$$

where $({}^{\mathcal{I}} p_{\mathcal{B}}, {}^{\mathcal{I}} R_{\mathcal{B}})$ denotes the origin and orientation of the *base frame* expressed in the inertial frame, and q_j denotes the *joint angles*. It is possible to define an operation associated with the set $\mathbb{Q}$ such that this set is a group. More precisely, given two elements q and ρ of the configuration space, the set $\mathbb{Q}$ is a group under the following operation:

$$q \cdot \rho = (p_q + p_\rho, R_q R_\rho, q_j + \rho_j). \tag{1}$$

Being the direct product of Lie groups, the set $\mathbb{Q}$ is itself a Lie group. The *velocity* of the multi-body system can then be characterized by the *algebra* $\mathbb{V}$ of $\mathbb{Q}$ defined by: $\mathbb{V} = \mathbb{R}^3 \times \mathbb{R}^3 \times \mathbb{R}^n$. An element of $\mathbb{V}$ is then a triplet

$$\nu = ({}^{\mathcal{I}}\dot{p}_{\mathcal{B}}, {}^{\mathcal{I}}\omega_{\mathcal{B}}, \dot{q}_j),$$

where ${}^{\mathcal{I}}\omega_{\mathcal{B}}$ is the angular velocity of the base frame expressed w.r.t. the inertial frame, i.e. ${}^{\mathcal{I}}\dot{R}_{\mathcal{B}} = S({}^{\mathcal{I}}\omega_{\mathcal{B}}){}^{\mathcal{I}}R_{\mathcal{B}}$.

Although the above digression on the robot configuration space may sound pedantic and marginal, let us observe that the choice of the group operation in (1) implies that an element $\nu \in \mathbb{V}$ is composed of $\dot{p}$, i.e. the time derivative of the origin of the floating base frame. Other choices for the group operation would imply a different algebra and, consequently, a different representation of the system's *velocity*.

We also assume that the robot is interacting with the environment through n_c distinct contacts. Applying the Euler-Poincaré formalism [1, Ch. 13.5] to the multi-body system yields the following equations of motion:

$$M(q)\dot{\nu} + C(q,\nu)\nu + G(q) = B\tau + J^{\top}(q)f \tag{1a}$$

$$J^{\top}(q)f := \sum_{k=1}^{n_c} J_{\mathcal{C}_k}^{\top} f_k \tag{1b}$$

where $M \in \mathbb{R}^{n+6\times n+6}$ is the mass matrix, $C \in \mathbb{R}^{n+6\times n+6}$ is the Coriolis matrix, $G \in \mathbb{R}^{n+6}$ is the gravity term, $B = (0_{n\times 6}, 1_n)^{\top}$ is a selector matrix, τ are the internal actuation torques, and f_k denotes an external wrench applied by the environment on the link of the k-th contact. We assume that the application point of the external wrench is associated with a frame $\mathcal{C}_k$, which is attached to the robot's link where the wrench acts on and has its z axis pointing as the normal of the contact plane. Then, the external wrench f_k is expressed in a frame whose orientation coincides with that of the inertial frame $\mathcal{I}$, but whose origin is the origin of $\mathcal{C}_k$, i.e. the application point of the external wrench f_k. The Jacobian $J_k = J_k(q)$ is the map between the robot's velocity ν and the linear and angular velocity ${}^{\mathcal{I}}v_{\mathcal{C}_k} := ({}^{\mathcal{I}}\dot{p}_{\mathcal{C}_k}, {}^{\mathcal{I}}\omega_{\mathcal{C}_k})$ of the frame $\mathcal{C}_k$, i.e.

$${}^{\mathcal{I}}v_{\mathcal{C}_k} = J_{\mathcal{C}_k}(q)\nu. \tag{2}$$

The Jacobian has the following structure.

$$J_{\mathcal{C}_k}(q) = \begin{bmatrix} J^b_{\mathcal{C}_k}(q) & J^j_{\mathcal{C}_k}(q) \end{bmatrix} \in \mathbb{R}^{6\times n+6}, \tag{2a}$$

$$J^b_{\mathcal{C}_k}(q) = \begin{bmatrix} 1_3 & -S({}^{\mathcal{I}}p_{\mathcal{C}_k} - {}^{\mathcal{I}}p_{\mathcal{B}}) \\ 0_{3\times 3} & 1_3 \end{bmatrix} \in \mathbb{R}^{6\times 6}. \tag{2b}$$

Lastly, we assume that rigid contacts may occur between the robot and the environment. The rigid contacts are assumed to be due to the rubbing of two flat surfaces belonging to the robot and to the environment, respectively. The constraint associated with the rigid contact is modeled as a kinematic constraint that forbids any motion of the frame $\mathcal{C}_k$, i.e. $J_{\mathcal{C}_k}(q)\nu = 0$.

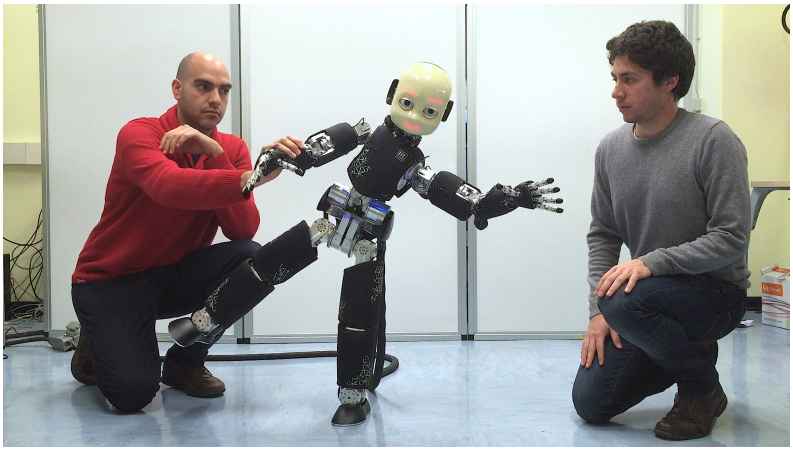

Figure 1: A screen-shot of the one-foot balancing demo

2.3 The controller for the first and second year validation scenario

The control objective for achieving balancing on either one foot or two feet has been the following ones since the beginning of the project:

1. Stabilization of the robot's momentum (expressed at the center-of-mass and with the inertial frame orientation), which is defined by

$$H = \sum H_i = \begin{pmatrix} m\dot{x} \\ H_\omega \end{pmatrix},$$

with H_i the momentum of each link composing the multi-body system, m the total mass of the robot, $x \in \mathbb{R}^3$ the position of the robot center-of-mass, and H_ω the angular momentum of the multi-body system. Let us recall that contrary to the case of a single rigid body, the possibility of expressing the angular momentum H_ω in terms of a proper angular velocity is still open. For this reason, we won't refer to a *robot angular velocity* when stabilizing the humanoid angular momentum.

The control of the robot momentum is achieved assuming the contact wrenches as a virtual control input in the dynamics of H. For instance, assuming that the robot is balancing on two feet, two external wrenches $f_L \in \mathbb{R}^6$ and $f_R \in \mathbb{R}^6$ act on the left and right foot, respectively. Then, one has

$$\dot{H} = mg + {}^c X_L f_L + {}^c X_R f_R = mg + \begin{pmatrix} {}^c X_L & {}^c X_R \end{pmatrix} f, \tag{3}$$

where ${}^c X_L, {}^c X_R \in \mathbb{R}^{6\times 6}$ are two proper projection matrices, and $f := (f_L^\top, f_R^\top)^\top$. Since f is assumed to be a control input, one can choose it so that $\dot{H} = \dot{H}^*$, where $\dot{H}^*$ ensures that $x \to x_d$ and $H_\omega \to 0$. Clearly, at this level, one is left with a six-dimensional redundancy of the control input. This redundancy is exploited to minimize joint torques.

2. In the null space of the above task, we want the robot to assume a desired joint configuration, while having also some compliance. This is achieved by means of a postural task at the joint torque level, which exploits a proportional-derivative plus gravity compensation control strategy for stabilizing a desired joint reference.

In the language of the *Optimization Theory*, the above control objectives can be formulated as follows.

$$f^* = \underset{f}{\operatorname{argmin}} |\tau^*(f)| \tag{4a}$$
$$s.t.$$
$$Cf < b \tag{4b}$$
$$\dot{H}(f) = \dot{H}^* \tag{4c}$$
$$\tau^*(f) = \underset{\tau}{\operatorname{argmin}} |\tau(f) - \tau_0(f)| \tag{5}$$
$$s.t.$$
$$\dot{J}(q,\nu)\nu + J(q)\dot{\nu} = 0 \tag{5a}$$
$$\dot{\nu} = M^{-1}(S\tau + J^\top(q)f - h(q,\nu)) \tag{5b}$$
$$\tau_0 = \bar{h} - \bar{J}_j^\top f - K_p(q_j - q_j^{des}) - K_d(\dot{q}_j - \dot{q}_j^{des}) \tag{5c}$$

For the sake of completeness, in the above optimization problem one has

$$\dot{H}^* = \begin{pmatrix} m(\ddot{x}_d - k_p(x - x_d) - k_d(\dot{x} - \dot{x}_d)) \\ -k_\omega H_\omega - k_i \int_0^t H_\omega ds \end{pmatrix} \tag{6a}$$
$$\bar{h} := h_j - M_{bj}^\top M_b^{-1} h_b \tag{6b}$$
$$\bar{h} := \begin{pmatrix} h_b \\ h_j \end{pmatrix} = C(q,\nu)\nu + G(q), \quad h_b \in \mathbb{R}^6 \quad h_j \in \mathbb{R}^n \tag{6c}$$
$$\bar{J} := J_j - J_b^\top M_b^{-1} M_{bj} \tag{6d}$$
$$M = \begin{pmatrix} M_b & M_{bj} \\ M_{bj}^\top & M_j \end{pmatrix} \quad M_b \in \mathbb{R}^{6\times 6} \quad M_{bj} \in \mathbb{R}^{6\times n} \quad M_b \in \mathbb{R}^{n\times n} \tag{6e}$$

Note that the additional constraint (4b) ensures that the desired contact wrenches f belong to the associated friction cones. Once the optimum f^* has been determined, the input torques τ are obtained by re-using the expression (5), i.e.

$$\tau = \tau^*(f^*) \tag{7}$$

Now, by direct calculations one can verify that the solution to the problem (5) is an affine function versus the desired wrenches f, i.e. $\tau^* = A(q,\nu)f + b(q,\nu)$, where $A \in \mathbb{R}^{n\times 12}$ and $b \in \mathbb{R}^n$ two proper matrices. This leads to the following simplification of the optimization problem

$$f^* = \underset{f}{\operatorname{argmin}} |\tau^*(f)| \tag{8a}$$
$$s.t.$$
$$Cf < b \tag{8b}$$
$$\dot{H}(f) = \dot{H}^* \tag{8c}$$
$$\tau^*(f) = A(q,\nu)f + b(q,\nu) \tag{8d}$$

The above control algorithm has run at both review meetings of the CoDyCo project.

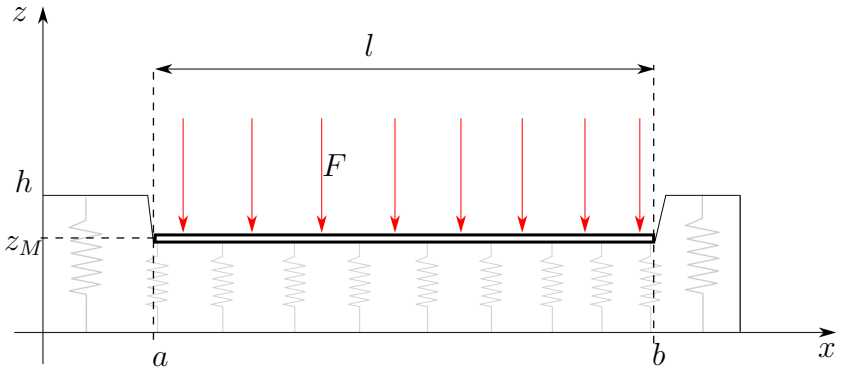

Figure 2: A compliant carpet subject to a uniform force distribution

3 Modelling and control design for a humanoid balancing on a thin carpet

This section discusses the modification of the control algorithm (4) for dealing with compliant contacts. Prior to the control design, however, we present a simple model for the carpet.

3.1 Modelling

To introduce the reader to the model of a compliant carpet, we first consider the planar case, and then address the three-dimensional case.

3.1.1 A case study: the planar case

Figure 2 shows a uniform force distribution acting on a compliant carpet of height h. The resultant force due to the distribution is denoted by F. The force distribution induces a compression of the compliant carpet and, assuming uniform carpet characteristics, the compression is equally distributed. So, the carpet is horizontal even after the compression due to the force distribution. Now, assume that the mapping $F : z_M \to F_E$ is known – or properly estimated – in the case shown in Figure 2. The following details how to evaluate the resultant force and torque acting from the carpet to the contact surface when it is not uniformly compressed. To this purpose, we make the following assumptions.

Assumption 1. *Throughout the paper, we assume the following.*

1. *The carpet characteristics are isotropic.*
2. *The soft carpet can be approximated as a continuum of springs. In addition, each infinitesimal spring can exert only a vertical force.*
3. *An off-line estimation procedure provides us with the mapping $F = F_E(z_M)$ when a uniform force distribution $f(\cdot)$ is applied to the carpet.*

Let l denote the length of the compliant carpet subject to the uniform force distribution. As a consequence of assumptions 1.1 and 1.3, one has:

$$F_E(z_M) = \int_a^b f(z_M)dx = f(z_M)l. \tag{9}$$

So, we can evaluate the force distribution $f(z)$ from the estimated force $F_E(z_M)$,

$$f(z) = \frac{F_E(z)}{l}. \tag{10}$$

Then, Eq. (9) can be used to evaluate the total force applied from the carpet to a generic contact surface, i.e.

$$F = \int_a^b f(z(x))dx, \tag{11}$$

with $z(x)$ a proper function describing the shape of the contact surface on a domain $x \in [a, b]$. Also, in view of the assumption 1.2, the torque about a point located at $x = \bar{x}$ of the carpet can be easily computed as:

$$M = \int_a^b f(z(x))(x - \bar{x})dx. \tag{12}$$

3.1.2 The case of a flat contact surface and a linear force distribution

Assume that the flat surface in Figure 2 bends as shown in Figure 3. Then, its shape can be characterized by a line of slope $\tan(\theta)$, i.e

$$z(x) = z_M + \tan(\theta)(x - x_M), \tag{13}$$

with (x_M, z_M) the coordinates of the central point of the flat plate. In addition, assume also that the estimated force $F = F_E(z_M)$ is linear with respect to the carpet's compression, i.e.

$$F_E(z_M) = K(h - z_M),$$

which implies

$$f(z) = k(h - z), \tag{14}$$

with $k := K/l$. Then, the total force and torque exerted from the compliant carpet to the flat surface is given by (11) and (12) evaluated with (14) and (13), i.e.

$$F = \int_{x_M - \frac{l}{2}\cos(\theta)}^{x_M + \frac{l}{2}\cos(\theta)} f(z(x))dx = kl\cos(\theta)\,(h - z_M) \tag{15a}$$

$$\begin{aligned} M &= \int_{x_M - \frac{l}{2}\cos(\theta)}^{z_M + \frac{l}{2}\cos(\theta)} f(z(x))(x - \bar{x})dx \\ &= kl\cos(\theta)\left[(h - z_M)\,(x_M - \bar{x}) - \frac{l^2}{12}\sin(\theta)\cos(\theta)\right] \end{aligned} \tag{15b}$$

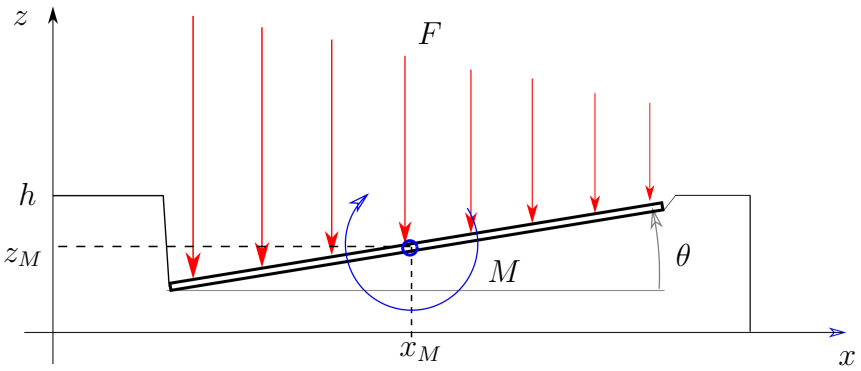

Figure 3: A compliant carpet subject to a non-uniform force distribution

The process of finding the solutions to the above integral is simplified by applying the variable transformation $\xi = x - x_M$, which renders the limits of integration equal to $-0.5l\cos(\theta)$ and $0.5l\cos(\theta)$. This hint is used for calculating the integrals in the more-complex 3-D case.

Note that if the torque M is expressed with respect to the central point (x_M, z_M) of the plate, one has:

$$F = kl\cos(\theta)\,(h - z_M) \tag{16a}$$

$$M = -k\frac{l^3}{12}\sin(\theta)\cos^2(\theta) \tag{16b}$$

As shown in Figure 3, positive angles θ produce negative torques,

3.1.3 The three-dimensional case

Analogously to the planar case, this section addresses the modeling of the forces and torques applied from a compliant carpet to a contact surface by considering the three-dimensional case. To this purpose, we still assume that Assumption 1 holds, modulo straightforward modifications for handling the three-dimensional case. In particular, we assume that an estimation procedure is performed when the contact surface is a flat, rectangular plate of length l and width d – see Figure 4. In addition, we also assume that the estimation procedure consists of applying a uniform force distribution so that the flat plate compresses the carpet uniformly. Hence, the estimated force takes the following form:

$$F_E(z) = e_3 \int_{x_0}^{x_1}\int_{y_0}^{y_1} f(z)dxdy = f(z)lde_3, \tag{17}$$

with $f(z)$ the vertical force distribution per surface. Hence, the force distribution can be evaluated as follows:

$$f(z) = \frac{|F_E(z)|}{ld}. \tag{18}$$

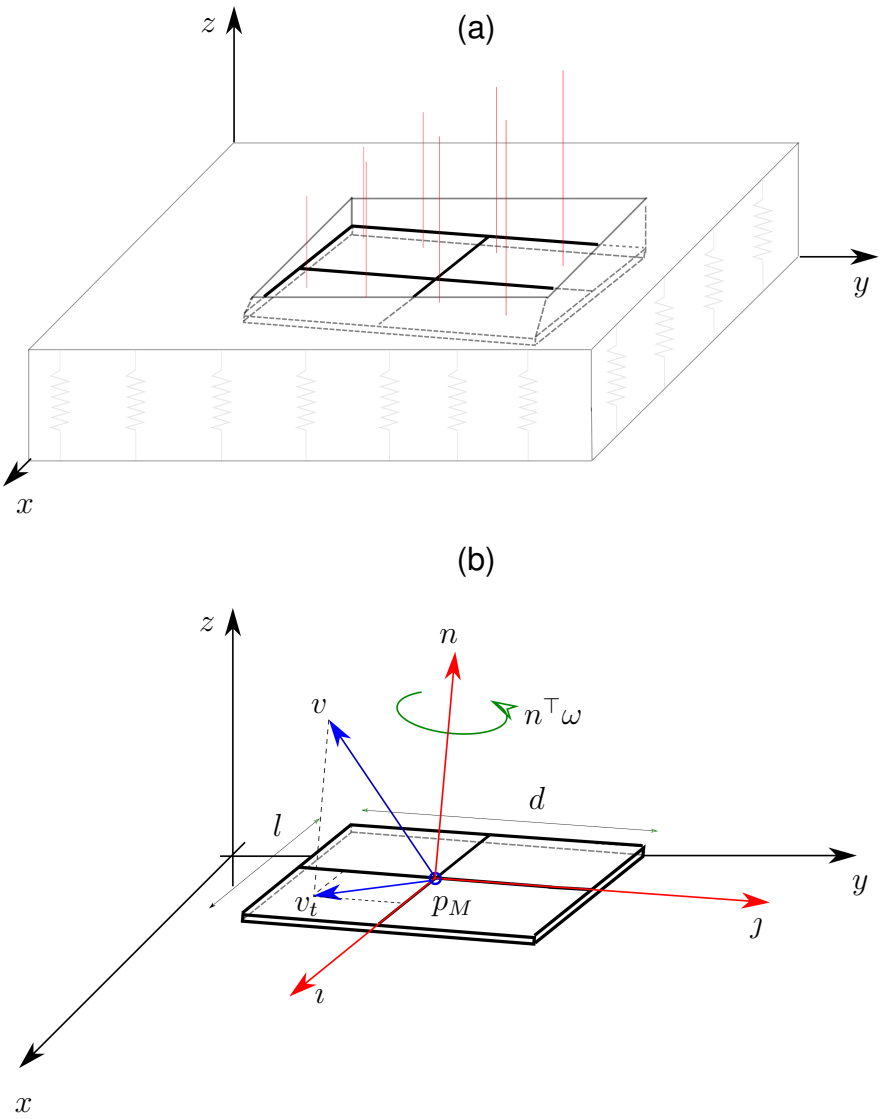

Figure 4: A compliant carpet subject to a non-uniform force distribution

In light of the above, the force and torque due to a generic contact surface is given by:

$$F = e_3 \int\int_D f(z)dxdy, \tag{19a}$$

$$M = \int\int_D f(z)S(p-\bar{p})e_3 dxdy, \tag{19b}$$

with $p = (x \quad y \quad z)^\top$ a point of the contact surface, $\bar{p} = (\bar{x} \quad \bar{y} \quad \bar{z})^\top$ the point w.r.t. which the torque is expressed, and $D \subset \mathbb{R}^2$ a proper integration domain associated with the contact surface configuration.

3.1.4 The case of a flat contact surface and a linear force distribution

Assume that the contact surface is flat – see Figure 4 – so it can be characterized by the following equation

$$n^\top p = 0, \tag{20}$$

with $n \in \mathbb{R}^3$ the unit vector perpendicular to the surface.

Lemma 1. *Assume that Assumption 1 holds, and that the force distribution $f(\cdot)$ associated with the compliant carpet is linear with respect to the height, i.e.*

$$f(z) = k(h - z). \tag{21}$$

Let a flat, rectangular surface, of length l and width d, be in full-contact with the compliant carpet. Then, the force-torque acting on the rectangular surface at the equilibrium configuration is given by:

$$F = kld|n^\top e_3|\,(h - z_M)\,e_3 \tag{22a}$$

$$M = S(p_M - \bar{p})F + \frac{kld}{12}|n^\top e_3|S(e_3)\Lambda(\imath, \jmath)e_3 \tag{22b}$$

with

$$\Lambda = d^2\jmath\jmath^\top + l^2\imath\imath^\top, \tag{23}$$

p_M the central point of the rectangular surface, and $\imath$ and $\jmath$ two unit, perpendicular vectors parallel to the rectangle's borders associated with the length and the width, respectively.

The proof is given in the Appendix. The above Lemma points out that the total force F depends on the normal n to the plane representing the flat plate, but it does not depend on the angle about this normal (i.e. the *yaw* angle about the normal n). Clearly, the force F also depends on how much the plate immerses into the soft carpet, and this dependence comes from the term $(h - z_M)$ in Eq. (22a). The expression of the torque M, instead, is the sum of two terms: the torque due to the force F applied at the point $\bar{p}$ plus a term depending only on the relative orientation of the plate w.r.t. the inertial frame. Note that if the plate is parallel to the plane $x - y$ of the inertial frame, then $\imath^\top e_3 = 0$ and $\jmath^\top e_3 = 0$. As a consequence, the second term on the right hand side of (22) is equal to zero, and so is the momentum M when expressed with respect to p_M (i.e. $\bar{p} = p_M$).

3.1.5 Constraints associated with the flat plate due to friction

Consider Figure 4, where $v \in \mathbb{R}^3$ denotes the velocity of the point p_M, and $\omega \in \mathbb{R}^3$ the angular velocity of the flat plate, both expressed with respect to the inertial frame. Then, it is reasonable to assume that friction effects forbid any rotation of the plate about the axis n as long as friction forces belong to the associated friction cones, i.e. $n^\top\omega = 0$. In addition, it is also reasonable to assume that friction effects forbid the

velocity of any point of the plate to be tangential to the plate itself. It is straightforward to verify that the velocity of any point p of the flat plate has null tangential velocity if and only if the velocity of the point p_M has null tangential velocity when $n^\top \omega = 0$. In light of the above, we assume that as long as friction forces belong to the associated friction cones, one has:

$$\imath^\top v = 0 \tag{24a}$$

$$\jmath^\top v = 0 \tag{24b}$$

$$n^\top \omega = 0 \tag{24c}$$

The above equations point out that the flat plate can rotate only about the axes $\imath$ and $\jmath$, and can also go "up-and-down" due to the compliance of the carpet. When coming to practice, however, it is also reasonable to assume that the vertical speed of the point p_M is equal to zero, i.e.

$$e_3^\top v = 0 \tag{25}$$

Let us justify this additional hypothesis. Eq. (22a) shows that the vertical force at the equilibrium configuration exerted from the carpet to the plate is given by

$$F_z = kld|n^\top e_3| \left(h - z_M\right).$$

Now, without loss of generality, assume that the point p_M is the plate's center of mass. Then, the force balance along the z axis writes:

$$m_p \ddot{z}_M = -k_v \dot{z}_M + kld|n^\top e_3| \left(h - z_M\right) - m_p g$$

where m_p is the mass of the plate, and k_v the viscous coefficient associated with the compliant carpet. In particular, thin compliant carpet are typically associated with very high value of k_v, which implies fast convergence of the plate vertical velocity to zero, i.e. $\dot{z}_M \to 0$. Also, from the above equation, it is clear that at the equilibrium configurations with a flat plate almost parallel to the ground, i.e. $|n^\top e_3| \approx 1$, one has

$$z_M \approx h - \frac{m_p g}{kld}.$$

Since the weight of the plate is constant, then the height z_M converges to the same value independently of an external, vanishing perturbation applied to the plate. This fact combined with the high value of carpet's damping justify the assumption (25).

3.1.6 Kinematic constraints and contact forces associated with the robot's feet

Assume that the robot is balancing on both feet, underneath which there is the compliant carpet characterized by the equations presented above. In view of Eq. (24)-(25), the constraints acting on both feet can be compactly written as:

$$\bar{H}^{\mathcal{I}} v_f = 0, \tag{26}$$

with

$$\bar{H} = \begin{pmatrix} H(\imath_L, \jmath_L, n_L) & 0_{4\times 6} \\ 0_{4\times 6} & H(\imath_R, \jmath_R, n_R) \end{pmatrix} \tag{27a}$$

$$v_f = \begin{pmatrix} \boldsymbol{v}_L \\ \boldsymbol{v}_R \end{pmatrix}, \tag{27b}$$

and $(\imath_L, \jmath_L, n_L)$ and $(\imath_R, \jmath_R, n_R)$ two frames attached to the left and right foot, respectively (as indicated in Figure (4)b and $\boldsymbol{v}_L$ and $\boldsymbol{v}_R$ the linear and angular velocity of the central point of the robot's feet, respectively. Now, the feet velocity ${}^{\mathcal{I}}v_f$ can be expressed in terms of the robot velocity ν though its Jacobian, i.e.

$${}^{\mathcal{I}}v_f = J(q)\nu.$$

By substituting the above equation into (26), one obtains

$$J_s(q)\nu = 0 \tag{28a}$$

$$\dot{J}_s(q)\nu + J_s(q)\dot{\nu} = 0 \tag{28b}$$

where

$$J_s(q) := \bar{H}(q)J(q). \tag{29}$$

Hence, the constraint equations when the robot stands on a compliant carpet have the same form of those when standing on rigid constraints (compare Eqs. (28) and (5a)). What does change between these two situations is the number of rigid constraints acting on the system. In fact, in the case the robot stands on rigid contacts, one has 12 kinematic constraints, while when the humanoid balances on the soft carpet, one has 8 rigid constraints acting on the system.

The rigid constraints generate eight contact *forces* $f^{rigid} \in \mathbb{R}^8$, which must be taken into account in the dynamic equation, i.e.

$$M(q)\dot{\nu} + C(q,\nu)\nu + G(q) = B\tau + J_s^{\top}(q)f^{rigid} + J^{\top}(q)f^{comp} \tag{30}$$

By combining the above equation with the constraints (28), one can find an expression of the contact forces f^{rigid}, which thus depend on the torque τ, and can be assumed as an artificial control input. Note that the effect of the compliant forces f^{comp} in Eq. (30) is also taken into account. Let $f_L^{comp} \in \mathbb{R}^6$ and $f_R^{comp} \in \mathbb{R}^6$ denote the compliant wrenches acting on the left and right foot, respectively. Assuming that the contact torques M in Eq. (22) are expressed w.r.t. the feet central point, i.e. $\bar{p} = p_M$, and that the feet can be approximated as two rectangles of the same dimension, one has

$$f_{comp} = \begin{pmatrix} f_L^{comp} \\ f_R^{comp} \end{pmatrix} = kld \begin{pmatrix} |n_L^{\top}e_3| \left(h - z_M^L\right) e_3 \\ \frac{1}{12}|n_L^{\top}e_3| S(e_3)\Lambda(\imath_L, \jmath_L)e_3 \\ |n_R^{\top}e_3| \left(h - z_M^R\right) e_3 \\ \frac{1}{12}|n_R^{\top}e_3| S(e_3)\Lambda(\imath_R, \jmath_R)e_3, \end{pmatrix} \tag{31}$$

with z_M^L and z_M^R the third components of the position vectors p_M^L and p_M^R describing the central points of the feet, i.e. $z_M^L = e_3^{\top}p_M^L$ and $z_M^R = e_3^{\top}p_M^R$.

3.2 Control design

Recall that the control objective is the asymptotic stabilization of the robot momentum, the rate of change of which equals the net external wrench acting on the system. In the case the robot is balancing on the compliant carpet described in Section (3.1.4), one then has

$$\dot{H}(f^{rigid}) = mg + \begin{pmatrix} {}^cX_L, & {}^cX_R \end{pmatrix} (\bar{H}^\top(q) f^{rigid} + f^{comp}), \tag{32}$$

where f^{rigid}, being dependent on the input torques τ, can be assumed as a control input in the above dynamics.

In light of the above, the control problem (4) is modified as follows to deal with the compliant carpet.

$$\begin{aligned}
f_*^{rigid} = & \underset{f^{rigid}}{\operatorname{argmin}} |\tau^*(f^{rigid})| && \text{(33a)}\\
& s.t. \\
& \quad C f^{rigid} < b && \text{(33b)}\\
& \quad \dot{H}(f^{rigid}) = \dot{H}^* && \text{(33c)}\\
& \quad \tau^*(f^{rigid}) = \underset{\tau}{\operatorname{argmin}} |\tau(f^{rigid}) - \tau_0(f^{rigid})| && \text{(34)}\\
& \qquad s.t. \\
& \qquad \quad \dot{J}_s(q,\nu)\nu + J_s(q)\dot{\nu} = 0 && \text{(34a)}\\
& \qquad \quad \dot{\nu} = M^{-1}(S\tau + J_s^\top(q) f^{rigid} + J^\top(q) f^{comp} - h(q,\nu)) && \text{(34b)}\\
& \qquad \quad \tau_0 = \bar{h} - \bar{J}_j^\top (\bar{H}^\top(q) f^{rigid} + f^{comp}) - K_p(q_j - q_j^{des}) - K_d(\dot{q}_j - \dot{q}_j^{des}) && \text{(34c)}
\end{aligned}$$

Analogously to what we discussed in Section 2.3, the above control problem is equivalent to:

$$\begin{aligned}
f_*^{rigid} = & \underset{f^{rigid}}{\operatorname{argmin}} |\tau^*(f^{rigid})| && \text{(35a)}\\
& s.t. \\
& \quad C f^{rigid} < b && \text{(35b)}\\
& \quad \dot{H}(f) = \dot{H}^* && \text{(35c)}\\
& \quad \tau^*(f) = A(q,\nu)(\bar{H}^\top(q) f^{rigid} + f^{comp}) + b(q,\nu) && \text{(35d)}
\end{aligned}$$

and once the optimal solution f_*^{rigid} is determined, we apply again Eq. (36) to determine the input torques to the robot.

The above control algorithm will be implemented for the third year demo review meeting when the humanoid must balance on two feet and on a compliant carpet.

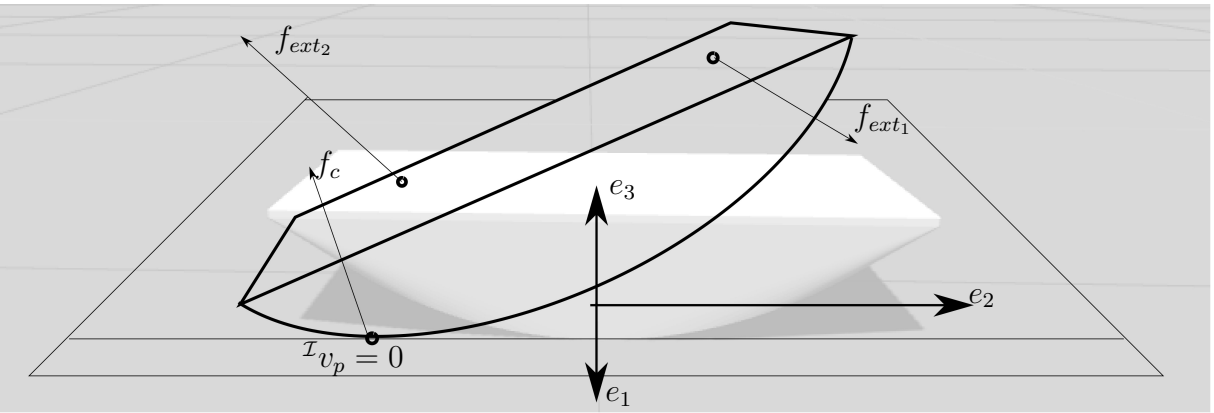

Figure 5: The semi-cylindrical seesaw

4 Control design for humanoids balancing on seesaws

4.1 The equation of motion of the seesaw

The equation of motion of the seesaw are derived by considering it as a rigid body subject to the rolling constraint. Let m_s and I_s denote the mass and the inertia matrix of the seesaw, and ${}^{\mathcal{I}}v_s$ and ${}^{\mathcal{I}}\omega_s$ the linear velocity of its center of mass and its angular velocity, respectively. Then, the momentum of the seesaw $H_s \in \mathbb{R}^6$ is defined by

$$H_s := \begin{pmatrix} m_s\, {}^{\mathcal{I}}v_s \\ I_s\, {}^{\mathcal{I}}\omega_s \end{pmatrix}, \tag{36}$$

and the equation of motion are given by

$$\dot{H}_s = \sum_i f_{ext_i} \tag{37}$$

subject to the following constraints

$$ {}^{\mathcal{I}}v_p = 0. \tag{38a}$$
$$ {}^{\mathcal{I}}\omega_s{}^{\top} e_2 = 0 \tag{38b}$$
$$ {}^{\mathcal{I}}\omega_s{}^{\top} e_3 = 0 \tag{38c}$$

with f_{ext_i} the external wrenches acting on the seesaw (see Figure 5). The kinematic constraints (38) express the following facts:

- The seesaw cannot rotate about the axes e_2 and e_3 of the inertial frame.
- The contact point between the seesaw and the floor possesses null velocity. This, along with the constraints on the seesaw angular velocity, ensures that all points of the contact line between the seesaw and the floor have zero velocity.

The satisfaction of the above constraints is ensured as long as the contact wrench w_c (see Figure 5) belong to the associated friction cones.

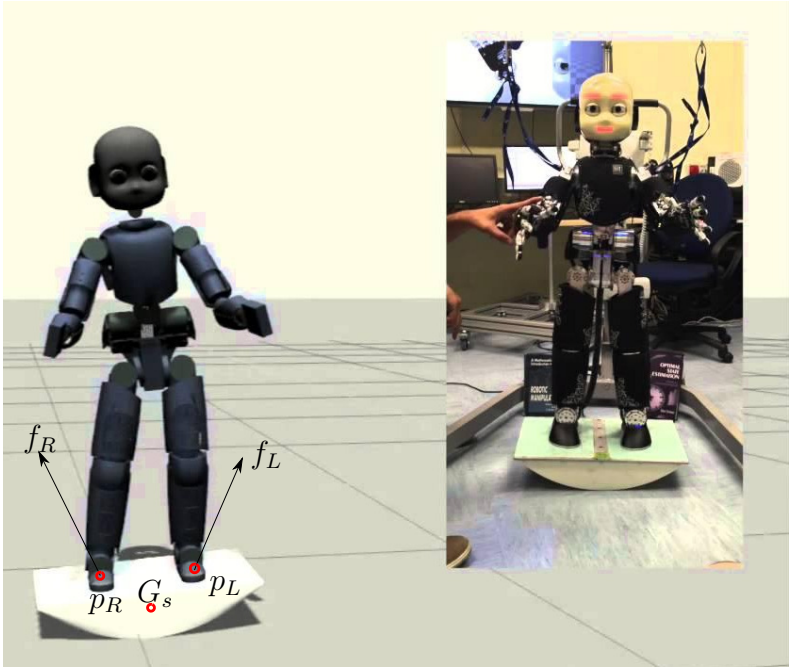

Figure 6: The robot balancing on the semi-cylindrical seesaw

4.2 Control design

Consider the robot balancing on the seesaw depicted in Figure 6. Recall that the control objective is the asymptotic stabilization of the robot's momentum H, the rate-of-change of which equals the net external force acting on the system. In the case of the robot balancing on the seesaw, one has:

$$\dot{H} = mg + {}^c X_L f_L + {}^c X_R f_R = mg + \begin{pmatrix} {}^c X_L & {}^c X_R \end{pmatrix} f, \tag{39}$$

where ${}^c X_L, {}^c X_R \in \mathbb{R}^{6\times 6}$ are two proper projection matrices, and $f := (f_L^\top, f_R^\top)^\top$. Now, we consider the contact forces f as a virtual control input of the above system, which can then be chosen so as $\dot{H} = \dot{H}^*$. To determine the relation between the contact forces f and the input torques τ, we have to define the constraints acting on the system robot plus seesaw.

To do so, consider, for instance, the left foot. As long as the foot stays in contact with the seesaw, the angular acceleration of the foot equals the angular acceleration of the seesaw. Analogously, the linear acceleration of any point belonging to the foot's sole equals the acceleration of the corresponding point belonging to the seesaw. This latter condition can be imposed by considering one single point of the foot's sole. As a consequence, the feet constraints can be expressed as follows:

$$\dot{J}(q)\nu + J(q)\dot{\nu} = a_c \tag{40}$$

where

$$a_c = \begin{pmatrix} a_L \\ a_R \end{pmatrix} = \begin{pmatrix} \ddot{p}_L \\ {}^{\mathcal{I}}\dot{\omega}_s \\ \ddot{p}_R \\ {}^{\mathcal{I}}\dot{\omega}_s \end{pmatrix} \tag{41}$$

and a_L and a_R the linear accelerations of the points p_L and p_R, respectively. Note that the accelerations a_L and a_R can be expressed in terms of the acceleration of the seesaw center of mass G_s through the relation

$$\ddot{p}_L = {}^{\mathcal{I}}\dot{v}_s + {}^{\mathcal{I}}\dot{\omega}_s \times (p_L - G_s) + {}^{\mathcal{I}}\omega_s \times (\dot{p}_L - {}^{\mathcal{I}}v_s). \tag{42}$$

The accelerations $\dot{v}_s$ and $\dot{\omega}_s$ can be evaluated from the Newton-Euler equation of the seesaw. By considering Figure 6, one has

$$\begin{aligned} \dot{H}_s = \frac{d}{dt}\begin{pmatrix} m_s {}^{\mathcal{I}}v_s \\ I_s {}^{\mathcal{I}}\omega_s \end{pmatrix} &= m_s g + {}^{s}X_c f_c - {}^{s}X_L f_L - {}^{s}X_R f_R \\ &= m_s g + {}^{s}X_c f_c - \begin{pmatrix} {}^{s}X_L & {}^{s}X_R \end{pmatrix} f, \end{aligned} \tag{43}$$

The above balance has been written by considering the fact that the force-torque (at each contact) that the seesaw exerts on the robot is equal and opposite to the force-torque the robot exerts on the seesaw. In view of (40), (41), (42), (43), one has

$$\dot{J}(q)\nu + J(q)\dot{\nu}(\tau, f) = a_c(f) \tag{44}$$

In light of the above, the control problem (4) is modified as follows to deal with the dynamical contacts generated by the seesaw.

$$f^* = \underset{f}{\operatorname{argmin}} |\tau^*(f)| \tag{45a}$$

$$s.t.$$

$$Cf < b \tag{45b}$$

$$\dot{H}(f) = \dot{H}^* \tag{45c}$$

$$\dot{H}_s = \dot{H}_s(f, fc) \tag{45d}$$

$${}^{\mathcal{I}}v_p = 0. \tag{45e}$$

$${}^{\mathcal{I}}\omega_s{}^{\top} e_2 = 0 \tag{45f}$$

$${}^{\mathcal{I}}\omega_s{}^{\top} e_3 = 0 \tag{45g}$$

$$\tau^*(f) = \underset{\tau}{\operatorname{argmin}} |\tau(f) - \tau_0(f)| \tag{46}$$

$$s.t.$$

$$\dot{J}(q)\nu + J(q)\dot{\nu}(\tau, f) = a_c(f) \tag{46a}$$

$$\dot{\nu} = M^{-1}(S\tau + J^{\top}(q)f - h(q, \nu)) \tag{46b}$$

$$\tau_0 = \bar{h} - \bar{J}_j^{\top} f - K_p(q_j - q_j^{des}) - K_d(\dot{q}_j - \dot{q}_j^{des}) \tag{46c}$$

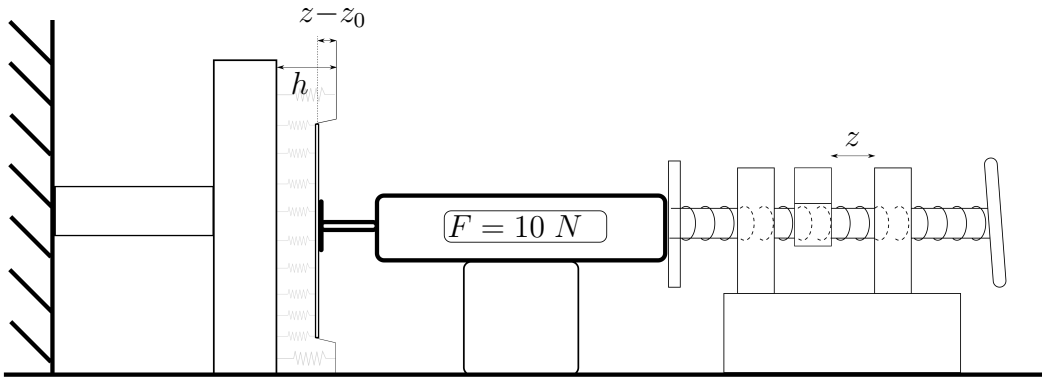

Figure 7: Estimation setup

5 Estimation algorithms

This section discusses the estimation algorithms for both the floating base and the compliance of the soft carpet.

5.1 Estimation of the floating base

5.2 Estimation of the floor compliance

This section presents preliminary results on the estimation of the force distribution $f(z)$ of the compliant carpet. The carpet's height is equal to $h = 1\ cm$.

5.3 The setup

Figure 7 shows the experimental setup used for estimating the compliance $f(z)$ associated with the chosen soft carpet. By means of a vise, we push a dynamometer that measures the force exerted from the compliant carpet to a flat plate attached to the dynamometer's top. The measurement of the carpet's compression is taken by using a high-precision caliper whose resolution is $0.01\ mm$.

5.4 Results

We carried on experiments with two rectangular contact surfaces of different size:

$S1:\ l_1 = 5.01\ cm$ and $d_1 = 2.01\ cm$;

$S2:\ l_2 = 5.6\ cm$ and $d_2 = 3.5\ cm$.

The measurements are taken so that the contact force spans the range $[0, 265]\ N$ for $S1$ and $[0, 388]\ N$ for $S2$. Figure 8 depicts both the measurements taken for the two

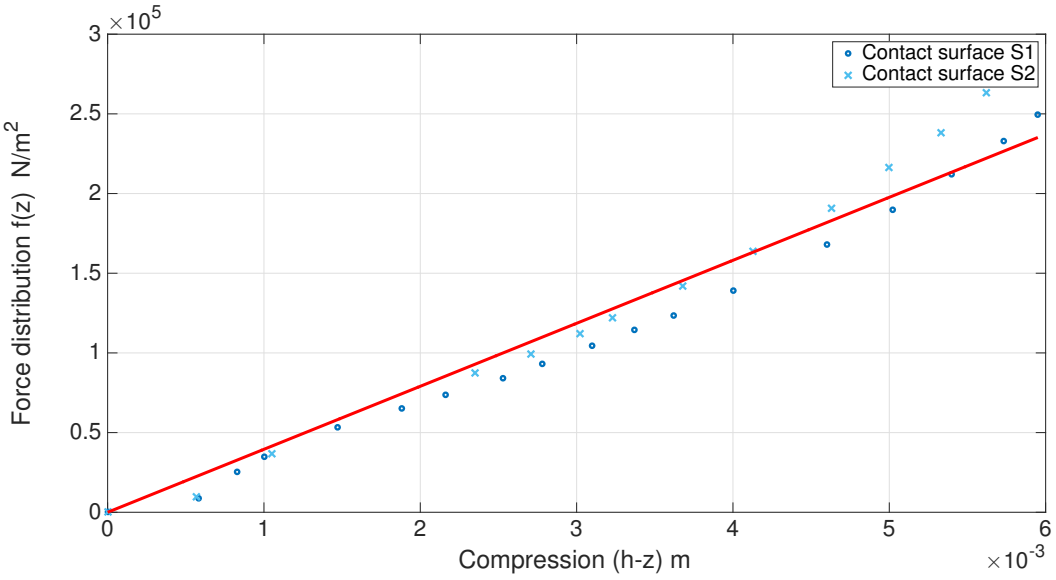

Figure 8: Estimation setup

different surfaces and the approximation result. Recall that the force distribution $f(z)$ is estimated from the measurement of the contact force via Eq. (18), i.e.

$$f(z) = \frac{|F_E(z)|}{l_i d_i},$$

with $i \in \{1, 2\}$. Hence, Figure 8 points out the following facts:

- Assumption 1.1, namely the carpet characteristics be uniform, is well-posed. In fact, measurements taken with a larger contact surface show that the governing behavior of the force distribution $f(z)$ does not change significantly versus the contact's surface.
- The assumption made in Lemma 1 on the linearity of the force distribution versus $(h - z)$ is well-posed.
- Since the carpet is of $h = 1\ cm$, it shows some nonlinear effects around $(h - z) \approx 0.6\ cm$. This threshold, which impairs the use of the model (21) to evaluate the total force-torque acting on the plate, is far from the operational condition representing a foot size in contact with the carpet.

References

[1] Marsden, J. E. and Ratiu, T. S. (2010). *Introduction to Mechanics and Symmetry: A Basic Exposition of Classical Mechanical Systems*. Springer Publishing Company, Incorporated.

Appendix

Proof of Lemma 1

First, note that any point $p = (x, y, z)$ of the rectangular surface can be expressed as follows

$$p = p_M + Rp', \tag{47}$$

where R is the rotation matrix given by $R = (\imath, \jmath, n)$, and $p' = (u, v, 0)$ any point of the rectangular surface expressed in the frame (p_M, R), which implies that $u \in \left[-\frac{l}{2}, \frac{l}{2}\right]$ and $v \in \left[-\frac{d}{2}, \frac{d}{2}\right]$. Then, we consider (47) as a variable change

$$x = x(u, v) \tag{48a}$$

$$y = y(u, v) \tag{48b}$$

to facilitate the process of finding the solutions to the integrals (19). Let us remind that given a double integral of a function $g(x, y) : \mathbb{R}^2 \to \mathbb{R}$, a variable change of the form (48) yields

$$\int\int g(x, y)dxdy = \int\int g(x(u, v), y(u, v))|\det(J)|dudv, \tag{49}$$

where J is the Jacobian of the variable transformation (48), i.e.

$$J = \begin{pmatrix} \partial_u x & \partial_v x \\ \partial_u y & \partial_v y \end{pmatrix} \tag{50}$$

It is straightforward to verify that the variable change (47) yields

$$|\det(J)| = |\imath_1\jmath_2 - \imath_2\jmath_1| = |n^\top e_3| \tag{51}$$

Once the variable change (48) has been applied, the domains on which the integrals (19) must be evaluated are normal with domains $u \in \left[-\frac{l}{2}, \frac{l}{2}\right]$ and $v \in \left[-\frac{d}{2}, \frac{d}{2}\right]$. Hence, from Eqs. (19) (21) (47) and (51), one has

$$F = e_3 k|n^\top e_3| \int_{-\frac{d}{2}}^{\frac{d}{2}} dv \int_{-\frac{l}{2}}^{\frac{l}{2}} (h - z_M - \imath_3 u - \jmath_3 v)du, \tag{52a}$$

$$M = k|n^\top e_3| \int_{-\frac{d}{2}}^{\frac{d}{2}} dv \int_{-\frac{l}{2}}^{\frac{l}{2}} (h - z_M - \imath_3 u - \jmath_3 v)S(p_M - \bar{p} + u\imath + v\jmath)e_3 du. \tag{52b}$$

By computing the above integrals, one gets (22).